International Journal of Biological Macromolecules 306 (2025) 141676

Contents lists available at ScienceDirect

International Journal of Biological Macromolecules

journal homepage: www.elsevier.com/locate/ijbiomac

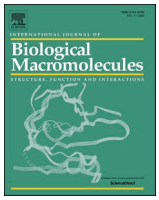

Tunning antisolvent precipitation for the synthesis of lignin nanoparticles using lignin extracted from different agro-industrial wastes

Ricardo Marchezan Farias de Mesquita [a], Willian Daniel Hahn Schneider [a], Vinicius Longo [a], Henrique Macedo Baudel [b], Eduardo Diebold [b], Jorge Rencoret [c], Ana Gutiérrez [c], Artur Cavaco-Paulo [d,e], Artur Ribeiro [d,e], Marli Camassola [a,*]

[a] Biotechnology Institute, University of Caxias do Sul, 95070-560 Caxias do Sul, RS, Brazil
[b] America Biomass Technologies, 02401-400 São Paulo, SP, Brazil
[c] Institute of Natural Resources and Agrobiology of Seville, CSIC, 41012 Seville, Spain
[d] CEB, Centro de Engenharia Biológica, Universidade do Minho, 4710-057 Braga, Portugal
[e] LABBELS, Associate Laboratory, Braga, /Guimarães, Portugal

ARTICLE INFO

Keywords:
Nanoprecipitation
Coconut
Sugarcane
Persimmon tree
Sustainability

ABSTRACT

Lignin nanoparticles (LNPs) show great potential in UV-protectants, drugs carriers, encapsulation, supercapacitors, and others. This study proposes the development of an optimised LNP synthesis method by antisolvent precipitation, using lignin from persimmon tree pruning waste, green coconut waste, and sugarcane bagasse. The best synthesis conditions were determined evaluating the chemical composition and the physicochemical properties of the LNPs, by varying the antisolvent addition rate, initial lignin concentration and antisolvent pH. Optimal precipitation conditions - 250 $\mu L \cdot s^{-1}$, 5 $mg \cdot mL^{-1}$ of lignin, pH 7.0 (antisolvent), 250 $\mu L \cdot s^{-1}$ adding antisolvent - converted the persimmon, coconut, and the sugarcane lignin into nanometric structures (Ø = 130–192 nm), with a spherical morphology, which were stable during storage at 5 °C for 90 days. Particle formation did not cause significant changes in the chemical composition of the lignins, and regardless of the plant origin, the LNPs showed higher UV absorption and thermal stability than the original corresponding lignins.

1. Introduction

Lignin is the second most abundant biopolymer in nature and the largest natural source of polyphenols, being composed of phenylpropanoid subunits that make up approximately 15–35 % of lignocellulosic biomass and provide structural rigidity to lignocellulosic materials [1–3]. Industrially, lignin is a by-product of pulp and paper production and second-generation ethanol in biorefineries, and due to its high calorific value has been explored as a solid fuel for the production of thermal energy [4,5]. Other properties such as thermal stability, oxidation resistance, ultraviolet (UV) radiation absorption, antioxidant activity, antibacterial activity, and good biocompatibility and biodegradability, makes lignin an attractive material for a variety of applications [5–10].

Although the availability and accessibility of lignins have increased with the development of new biorefineries, there are still some problems that hamper their reuse and valorisation [11,12]. Lignins are recalcitrant, have low water solubility, are heterogeneous, and show variability at structural level, depending on the source and methods used for the separation and pre-treatment of biomass [2,4].

Lately, lignins have been explored as polymer matrices for the synthesis of nanoparticles, taking advantage of their low solubility in water [3,13]. Lignin nanoparticles (LNPs) offer advantages over lignin, such as higher surface-to-volume ratio, better dispersion in an aqueous environment, better mechanical properties, and thermal stability, and higher antioxidant activity and UV absorption capacity [13–17]. Moreover, the residual materials of LNPs have no adverse effect on the target sites after their activity [6,18]. LNPs can also be chemically modified to acquire various features and applications, including for the encapsulating agents, to act as catalytic supports, and to be used as reinforcements for composites, among others [19,20].

Several techniques have been used for the synthesis of LNPs

* Corresponding author.
E-mail address: mcamasso@ucs.br (M. Camassola).

https://doi.org/10.1016/j.ijbiomac.2025.141676
Received 18 September 2024; Received in revised form 17 February 2025; Accepted 28 February 2025
Available online 1 March 2025

including ultrasonication, polymerization, interfacial crosslinking, and aerosol flow [3,13]. Despite their efficiency in particles formation, these processes require specific equipment and facilities, some of which are expensive, making their scale-up economically infeasible [21]. A practical and affordable alternative is antisolvent precipitation, which consists of adding a polar antisolvent, such as water, to an organic solvent containing dissolved lignin to induce the formation of colloidal lignin aggregates [13,22]. This method allows to control the size and morphology of the LNPs, and after synthesis, to recover the organic solvent used to solubilize the lignins [13]. However, to obtain LNPs using the antisolvent precipitation approach, it is necessary to adjust the process conditions, such as the amount of dissolved lignin, the choice of solvent/antisolvent, the pH, and the addition rate of the antisolvent [19,23]. Moreover, the plant source from which the lignin is extracted (different compositions) can alter the lignins potential to form LNPs and the properties of the particles [13,24].

The present study proposes to develop an optimised antisolvent precipitation methodology for the synthesis of LNPs, using lignins extracted from different vegetable raw materials – green coconut waste (green exocarp, fibrous mesocarp, and hard endocarp of *Cocos nucifera* L.), persimmon tree pruning waste (twigs and leaves of *Diospyros kaki* L. f.), and sugarcane bagasse (*Saccharum officinarum* L.). Green coconut waste is a material that cannot be returned to plantations because it accumulates water inside and contributes to mosquito proliferation and consequent transmission of diseases. Sugar cane bagasse, a biomass that is abundant in the southern hemisphere. Persimmon tree prunings, a fruit plant that needs to be pruned and these prunings leave behind diseases such as fungi, but the prunings are not removed from plantations because the labour to remove them is expensive [25]. So, it is necessary to look for alternatives to add value to these wastes. Furthermore, it is intended to evaluate how the lignins origin affects the particle synthesis process and the final properties of the new LNPs, such as morphology, chemical composition, colloidal stability, ultraviolet radiation absorption, and resistance to thermal degradation. While this work differs from previous studies, which have focused predominantly on lignin obtained from conventional sources, our research innovates by using regional agricultural waste, diversifying the raw material and proposing a sustainable route for utilising waste that contributes to reducing environmental impact.

2. Materials and methods

2.1. Biomass collection and preparation

Green coconuts (*Cocos nucifera* L.) were purchased from the Horticultural Products Supply Centre of Serra Gaúcha (Ceasa/Serra), in Caxias do Sul, Rio Grande do Sul, Brazil. The total green coconut waste, constituted by green exocarp, fibrous mesocarp (husk), and hard endocarp (shell), was cut into 10 cm fragments. Twigs and leaves of persimmon (*Diospyros kaki* L.f.) trees were collected during fruit pruning in February 2020 in Caxias do Sul, Brazil (−29.0931°S, −51.0893°W). The persimmon tree pruning waste contained 53 % (*w/w*) twigs and 47 % (*w/w*) leaves. The residues containing only leaves or twigs and the fraction containing both were cut into 15 cm pieces. Sugarcane bagasse was supplied by America Biomass Technologies. All the biomass was dehydrated at 50 ± 5 °C to 10 % humidity. Biomasses were then ground in a knife mill (Rone Mills, FA-2305) and fractionated by sieving. Samples of mesh sizes 24 to 48 were used to carry out the experiments.

2.2. Chemical characterization of the biomass

The lignocellulosic composition of untreated biomass was determined according to the National Renewable Energy Laboratory (NREL) methodology for proteins [26], extractives [27], ash [28], structural carbohydrates, and lignin [29].

2.3. Lignins extraction

Lignins were extracted from green coconut waste (green exocarp, fibrous mesocarp, and hard endocarp of *Cocos nucifera*), persimmon tree pruning waste (twigs and leaves of *Diospyros kaki*), and sugarcane bagasse (*Saccharum officinarum*) by acid-alkali treatment, acid precipitation, purification, and lyophilisation. The dried biomass, 10 % *(w/v)*, was subjected to diluted acid pre-treatment (DAP) with H_2SO_4 in 1 L flasks in sequential steps. In the first step, which lasts 60 min with distilled water, the second lasting 30 min both with 0.5 % *(w/w)* H_2SO_4, and the third lasting 15 min with 1.0 % *(w/w)* H_2SO_4. DAP conditions were carried out at 125 °C and 1.05 bar. The slurry was centrifuged at 3220 ×*g* for 20 min. The washing consisted of dispersing 5 % *(w/v)* of the pre-treated biomass in distilled water and mixing with a mechanical stirrer (Fisatom, 713DS) at 600 rpm for 1 h until the washing water reached a pH of 6.0–8.0. The biomass was then dried at 50 ± 5 °C. Alkaline treatment (AT) was performed on the pre-treated biomass. For AT, 5 % *(w/w)* of dry biomass with 2.0 % *(w/v)* NaOH was placed in 2 L flasks at 125 °C and 1.05 bar and was incubated for 60 min. The slurry was vacuum filtered, and the biomass was washed as described above. Lignin was recovered from the AT liquor by slowly adding H_2SO_4 (95 %) to pH 1.5–2.0. The suspension was centrifuged at 3220 ×*g* for 20 min. The lignins were then washed with acidified water at pH 2 and were lyophilised and stored at stored in plastic tubs with screw-top lids, hermetically sealed, and kept in a dark environment at room temperature.

2.4. Lignin nanoparticles synthesis

Lignin nanoparticles (LNPs) were obtained by precipitation using a mixture of 90 % (*v/v*) acetone, 6 % (*v/v*) ethanol, and 4 % (*v/v*) deionised water as the solvent and deionised water as the antisolvent. Lignin solutions of 1 to 20 $mg{\cdot}mL^{-1}$ were prepared by dissolving the lignins in acetone:ethanol:water 90:6:4 (*v:v:v*) (condition selected in initial tests) for 10 min at 600 rpm. After this period, the lignin solutions were filtered through a 0.45 μm nylon membrane to remove possible undissolved solids. The filtrate was then kept at room temperature (25 ± 5 °C) under magnetic stirring at 600 rpm. The antisolvent (pH 2–12) was added to the lignin solutions at a flow rate of 25–250 $\mu L{\cdot}s^{-1}$ using a peristaltic pump. Solutions of 0.1 mol/L NaOH and 0.05 mol/L H_2SO_4 were used to adjust the pH of the antisolvent. The lignin solution was stirred for 10 min before adding the antisolvent. When the 1:9 (*v/v*) ratio of antisolvent solution to lignin was reached, the addition of the antisolvent was stopped. The organic solvents were removed by rotary evaporation, and the LNPs were recovered by lyophilisation. The yield was expressed as the ratio of grams LNPs per gram of the initial process lignin.

After lyophilisation, the LNPs were stored in powder form, packed in plastic containers, protected from light, and kept at room temperature. For redispersion, the LNPs were mixed with distilled water and stirred for at least 10 min.

2.5. Lignins and lignin nanoparticles characterization

2.5.1. Dynamic light scattering (DLS)

The hydrodynamic diameter (HDD), dispersity (Đ), and zeta potential (ζ-potential) of the LNPs were determined by dynamic light scattering (DLS) using the Zeta Sizer Nano-ZS ZEN 3600 (Malvern, UK). All analyses were performed in triplicate.

2.5.2. Field emission scanning electron microscopy (FE-SEM)

FE-SEM micrographs were taken on a scanning electron microscope 3rd generation VEGA (Tescan Orsay Holding, CZ). The samples were sputtered onto gold using a magnetron sputtering device. The diameter of the LNPs was obtained by automatically measuring the particle size in the micrographs using TESCAN Essence™ software.

2.5.3. Pyrolysis-gas chromatography/mass spectrometry (Py-GC/MS)

The analytical pyrolysis of lignin and LNPs samples (~0.1 mg) was performed in a Frontier 3030 micro-furnace pyrolyser (Fukushima, Japan) coupled to an Agilent 7820 A GC/5975 mass-selective detector (Agilent Technologies Inc., USA). A DB-1701 capillary column (30 m × 0.25 mm ID, 0.25 μm film thickness) was used (J&W Scientific, USA). The pyrolysis was performed at 500 °C, and the GC oven temperature was programmed from 50 °C to 100 °C at 20 °C·min^{-1} and then ramped to 280 °C at a heating rate of 6 °C·min^{-1} and held for 5 min. The carrier gas was helium (1 mL·min^{-1}). The phenolic compounds released were identified by comparison of their mass spectra with those reported in the literature [30,31]. Peak molar areas for each lignin-derived phenolic compound were calculated, the summed areas were normalised, and the data from duplicate analyses were averaged and expressed as percentages.

2.5.4. Two-dimensional nuclear magnetic resonance (2D-NMR) spectroscopy

Lignin and LNP samples (~40 mg) were transferred into 5 mm NMR tubes and dissolved in 0.6 mL of deuterated dimethyl sulfoxide (DMSO-d_6). NMR spectra were acquired on a cryoprobe-equipped AVANCE III 500 MHz instrument (Bruker Corporation, USA). Two-dimension heteronuclear single quantum coherence (2D-HSQC) NMR spectra were acquired at 300 K using an adiabatic pulse sequence (hsqcetgpsisp.2) which enabled a semiquantitative analysis of the different ^{13}C—^{1}H correlation signals. Spectra were acquired from 10 to 0 ppm in F2 (^{1}H) using 1000 data points with an acquisition time of 145 ms, an interscan delay of 1 s, and from 170 to 0 ppm in F1 (^{13}C) using 256 increments of 32 scans, for a total experiment time of 2 h 34 min. The $^{1}J_{CH}$ coupling constant used was 145 Hz. HSQC spectra were processed using Bruker TopSpin 3.6 software and the following parameters: Gaussian apodisation in ^{1}H (LB = -0.1 and GB = 0.001) and a squared cosine bell in ^{13}C (LB = 0.3 and GB = 0.1). The residual DMSO central peak was used as an internal reference (δ_C/δ_H 39.5/2.49). HSQC cross-signals were assigned by literature comparison [30–32]. A semi-quantitative analysis of the volume integrals of the HSQC correlation peaks was performed using Bruker's Topspin 3.6 processing software. In the aromatic/unsaturated region, the correlation signals of G_2 and $S_{2,6}$ were used to estimate the content of the respective G- and S-lignin units (as the signal $S_{2,6}$ involves two proton-carbon pairs, its volume integral was halved). The signals used to quantitate the relative abundances of *p*-coumaric acid (*p*CA), ferulic acid (FA), *p*-hydroxybenzoic acid (*p*BA), and kaempferol (K) moieties were $pCA_{2,6}$, $FA_{2,}$ $pBA_{2,6}$, and K_6, respectively (the volume integrals of $pCA_{2,6}$ and $pBA_{2,6}$ were halved). The different inter-unit linkages were quantitated by the volume integrals of the A_α ($\beta - O - 4'$), B_α (β–5′), and C_α (β–β′) correlation signals corresponding to chemically analogous C_α/H_α with similar $^{1}J_{CH}$ coupling values.

2.5.5. Fourier-transform infrared spectroscopy (FT-IR)

FT-IR spectra of lignins and LNPs were acquired at room temperature on a Nicolet-Avatar 360 FT-IR spectrometer (Thermo Fisher Scientific Inc., USA) from 4000 to 400 cm^{-1} with a resolution of 32 cm^{-1}. The bands were analysed using OriginPro 8.5 software (OriginLab Corporation, USA).

2.5.6. LNPs stability assay

The stability of LNPs was evaluated by measuring the HDD, Đ, and ζ-potential in DLS during storage at 5 °C for 90 days.

2.5.7. Absorbance assay in ultraviolet-visible (UV–vis)

Dispersions of 0.05 mg·mL^{-1} lignin and LNPs were prepared in deionised water at pH 7 and stirred for 10 min, as adapted from Maldonado-Carmona et al. [33]. The samples were transferred to a 96-well synthetic quartz microplate (Hellma, Germany) and the absorbance was measured on a Bioteck Synergy H1M2 spectrophotometer (Agilent Technologies Inc., USA) between 230 and 700 nm at 5 nm intervals at 25 °C.

2.5.8. Thermal stability assay by thermogravimetric analysis (TGA)

Lignins and the corresponding LNPs (~4 mg) were heated from 30 to 800 °C at a heating rate of 10 °C·min^{-1}. Analysis was performed in a nitrogen atmosphere at a constant flow rate of 50 mL·min^{-1} in a TGA-50 thermal analyser (Shimadzu, Japan).

2.6. Statistical analysis

SPSS Statistics 20 was used for statistical analysis. Parametric data (Shapiro-Wilk test, $p \leq 0.05$) were expressed as the arithmetic mean ± standard error, and the significance between data was assessed using the independent samples test ($p \leq 0.05$) between two independent variables or ANOVA with Tukey's test ($p \leq 0.05$) for more than two independent variables. Non-parametric data (Shapiro-Wilk test, $p > 0.05$) were expressed as median ± standard deviation and significant differences between data were analysed using the Kruskal-Wallis test with the Dunnett test ($p \leq 0.05$).

3. Results and discussion

3.1. Biomass characterization

The chemical compositions of the lignocellulosic biomass samples used in this work are shown in Table 1A. Analysing the results, some variations can be identified regarding the concentration of lignin present in each biomass source. The perennial plants showed higher amount of lignin with ~28 % and coconut has ~24 %, while the sugarcane bagasse, a grass, showed the lowest percentage of lignin (~18 %).

3.1.1. Lignin characterization

The lignins isolated from green coconut waste, persimmon tree pruning waste, and sugarcane bagasse were of high purity, with a salmon colour, and presented a total lignin content of 90.4 ± 0.8 %, 97.2 ± 3.6 % and 97.4 ± 1.7 % (w·w^{-1}), respectively.

Besides the high selectivity of the acid-alkali treatment for protolignin, the washing cycles of the recovered lignin during purification might have contributed to this purity level. The composition of the different lignins was first analysed by Py-GC/MS. In all cases, pyrolysis released phenolic compounds derived from *p*-hydroxyphenyl (H), guaiacyl (G), and syringyl (S) lignin units (Table 1B). In all samples (Table 2), the major lignin-derived compounds released by pyrolysis were guaiacol (2), 3-methylphenol (4), 4-methylguaiacol (5), 4-syringol (11), 4-methylsyringol (14), 4-ethylsyringol (16), and 4-vinylsyringol (17). It is important to note that the high relative amounts of phenol (1) (in coconut lignin), 4-vinylphenol (9) and 4-vinylguaiacol (8) (in sugarcane lignin) are mainly derived from the *p*-hydroxybenzoates (*p*BA), *p*-coumarates (*p*CA), and ferulates (FA), respectively, which are decarboxylated during pyrolysis [31,34].

The analysis showed great differences in the composition of the lignins extracted from the different biomass. The lignin from the persimmon tree showed a high amount of S-lignin units, with an S/G ratio of 2.5, which is comparable to that found in hardwood lignins [13,35]. The lignin remaining from green coconut had almost equal proportions of S and G lignin units, resulting in an S/G ratio of 1.1, confirming previous studies with lignins from coconut fibre [31,36]. Because it was isolated from a herbaceous plant, sugarcane bagasse lignin contained compounds derived from all three types of lignin units but with a predominance of phenols from S and G units [13,37]. Py-GC/MS analysis also revealed the presence of significant amounts of fatty acids in the lignin fractions isolated from persimmon trees and green coconut waste, especially in the latter.

The HSQC spectra (δ_C/δ_H 50–147/2.5–8.2) of the different extracted lignins, together with the main structures identified, are shown in Fig. 1

Table 1
Chemical characterization of persimmon tree pruning waste, green coconut waste and sugarcane bagasse (A). Phenolic compounds identified from the pyrolysis products of the lignins extracted from persimmon tree pruning waste, green coconut waste, and sugarcane bagasse. Compounds abundances are expressed as relative percentages of molar areas (B).

(A)	Composition (%, *w/w*)	Persimmon tree	Green coconut	Sugarcane bagasse
	Proteins	7.37 ± 0.15	1.80 ± 0.07	1.01 ± 0.12
	Extractives	21.28 ± 0.87	20.70 ± 0.61	13.05 ± 0.66
	Extractives in water	16.58 ± 0.64	20.17 ± 0.71	12.22 ± 0.69
	Extractives in ethanol	4.65 ± 0.33	0.53 ± 0.11	0.72 ± 0.05
	Lignin	27.95 ± 0.44	23.76 ± 0.66	18.30 ± 0.45
	Acid insoluble lignin	24.53 ± 0.51	20.48 ± 0.65	15.30 ± 0.43
	Acid soluble lignin	3.42 ± 0.35	3.28 ± 0.09	3.00 ± 0.10
	Glucan	16.61 ± 0.16	22.36 ± 0.61	31.01 ± 2.36
	Xylan	8.52 ± 0.06	19.73 ± 0.60	13.81 ± 1.32
	Arabinan	1.97 ± 0.05	1.08 ± 0.06	2.03v ± 0.12
	Acetate	2.73 ± 0.24	4.35 ± 0.13	4.93 ± 0.33
	Ash	4.84 ± 0.34	2.18 ± 0.22	2.08 ± 0.08
	Total	91.25 ± 1.08	95.97 ± 1.27	86.22 ± 2.84

(B)	N.	Compound	Origin	Persimmon	Coconut	Sugarcane
	1	Phenol	*p*BA/H	3.9	15.9	3.3
	2	Guaiacol	G	10.5	13.4	6.5
	3	4-methylphenol	H	1.7	1.1	0.8
	4	3-methylphenol	H	5.3	10.0	3.5
	5	4-methylguaiacol	G	6.4	8.0	5.7
	6	4-ethylphenol	H	1.8	6.2	4.2
	7	4-ethylguaiacol	G	3.7	5.0	4.0
	8	4-vinylguaiacol	G/FA	7.0	6.2	11.5
	9	4-vinylphenol	H/*p*CA	2.8	1.6	25.1
	10	Eugenol	G	0.2	0.2	0.3
	11	Syringol	S	18.2	10.2	10.4
	12	*cis*-isoeugenol	G	0.2	0.2	0.3
	13	*trans*-isoeugenol	G	1.3	1.1	1.2
	14	4-methylsyringol	S	12.1	6.9	7.8
	15	Vanillin	G	–	–	0.4
	16	4-ethylsyringol	S	8.0	5.2	3.4
	17	4-vinylsyringol	S	10.3	4.0	3.1
	18	4-allylsyringol	S	0.6	0.4	0.4
	19	*cis*-4-propenylsyringol	S	0.8	0.6	0.5
	20	*trans*-4-propenylsyringol	S	2.5	1.7	1.5
	21	Syringaldehyde	S	–	–	1.4
	22	Acetosyringone	S	1.1	1.0	2.7
	23	Syringylacetone	S	1.6	0.9	1.9
			H (%)*	14.1	22.8	18.6
			G (%)*	24.8	36.7	29.1
			S (%)*	61.1	40.5	52.3
			S/G ratio	2.5	1.1	1.8

* H-units: in the case of the lignin extracted from green coconut waste, phenol (1) has been excluded from calculating the H-lignin units (%) as it mainly comes from *p*-hydroxybenazoates (*p*BA) decarboxylation. 4-vinylphenol (9) has been also excluded as it comes from *p*-coumarates decarboxylation. G-units: similarly, 4-vinylguaiacol (8) has been excluded from calculating the G-lignin units (%) as it comes from ferulates (FA) decarboxylation.

(a, b, and c). The main signals observed in the aromatic region of the HSQC spectra correspond to the aromatic rings of the different guaiacyl (G) and syringyl (S) lignin units, including Cα-oxidized S-lignin units (S′), as well as to the aromatic rings and the unsaturated side-chains of the *p*-hydroxycinnamates (*p*CA and FA) and *p*-hydroxybenzoates (*p*BA). *p*-Hydroxyphenyl (H) lignin units could not be clearly observed because their signals overlap with those from proteins. In the aliphatic-oxygenated region of the spectra, typical signals for the C_α/H_α, C_β/H_β, and C_γ/H_γ correlations of the different inter-unit linkages ($\beta - O - 4'$ alkyl-aryl ethers, A; β–5′ phenylcoumarans, B; β–β' resinols, C) were observed [30,31]. A semi-quantitative estimation of the main structural characteristics of the extracted lignins, such as the relative abundances of the different interunit linkages, the relative abundances of the lignin units (H, G, and S), and the S/G ratios estimated from volume integration of the signals in the HSQC spectra, are indicated in Table 2. The data show that the three lignins have a predominance of β–*O*–4′ aryl ether linkages (> 85 %). Persimmon tree lignin had a higher prevalence of β–β' resinol-type linkages, whereas β–5′ phenylcoumarans linkages were more prevalent in coconut and sugarcane lignins. The S/G molar ratios obtained by 2D-NMR were close to those determined by Py-GC/MS. Interestingly, the HSQC analysis revealed that the lignin extracted from sugarcane bagasse is enriched in free *p*-coumaric acid (most likely from hydrolysis, during the isolation process, of *p*-coumarates that acylate native sugarcane lignin) and indicated the presence of flavonoids such as kaempferol in the lignin extracted from persimmon tree. Furthermore, HSQC showed that only coconut lignin contains *p*-hydroxybenzoates (*p*BA).

Table 2
2D-HSQC NMR semiquantitative analysis of the lignin bonds and structural units, as well as FA, *p*CA, *p*BA, and kaempferol moieties in the lignins extracted from persimmon tree pruning waste, green coconut waste, and sugarcane bagasse.

Parameters	Persimmon	Coconut	Sugarcane
Linkages (%)*			
β–*O*–4′ alkyl aryl ethers (A)	85	89	89
β–5′ phenylcoumarans (B)	3	7	8
β–β' resinols (C)	12	4	3
Aromatic units			
H (%)	–	–	–
G (%)	28	45	31
S (%)	72	55	65
S/G ratio	2.6	1.2	2.1
Ferulates (FA)**	4	–	9
p-coumaric acid (*p*CA)**	1	1	27
p-hydroxybenzoates (*p*BA)**	–	8	–
Kaempferol (K)**	3	–	–

* Estimated as a percentage of the total linkages (A + B + C = 100).
** FA, *p*CA, *p*BA, and kaempferol contents as percentages of lignin content (H + G + S = 100).

The chemical composition and structural features of lignin, including molecular weight, functional groups, and degree of polymerization, significantly influence its self-assembly behavior and the resulting nanoparticle characteristics [38]. The monomeric composition, particularly the ratio of syringyl (S) to guaiacyl (G) units, plays a key role in determining the reactivity of lignin and the properties of derived nanoparticles. Lignins with a higher S content typically have fewer cross-links, which can lead to the formation of more uniform nanoparticles [5].

The presence of carboxyl and phenolic hydroxyl groups in lignin enhances its aqueous solubility, promoting the formation of stable lignin nanoparticle (LNP) dispersions in water [38]. Conversely, more hydrophobic lignins, characterized by fewer polar functional groups, may require surfactants or apolar solvents for effective nanoparticle synthesis. In contrast, hydrophilic lignins readily form LNPs in aqueous conditions.

Additionally, β-O-4 bonds in lignin increase the flexibility of its polymer chain and enhance the availability of functional groups, facilitating emulsification and the formation of smaller, more uniform LNPs. On the other hand, cross-links such as C—C and C-O-C bonds contribute to rigidity of lignin, which hinders its dissolution and subsequent self-organization into nanoparticles. Furthermore, the presence of quinone and keto-enolic groups can influence redox reactions or intermolecular interactions during nanoparticle formation, impacting the chemical stability and size of the resulting LNPs [3,39].

Furthermore, these data obtained indicates that the pre-treatment

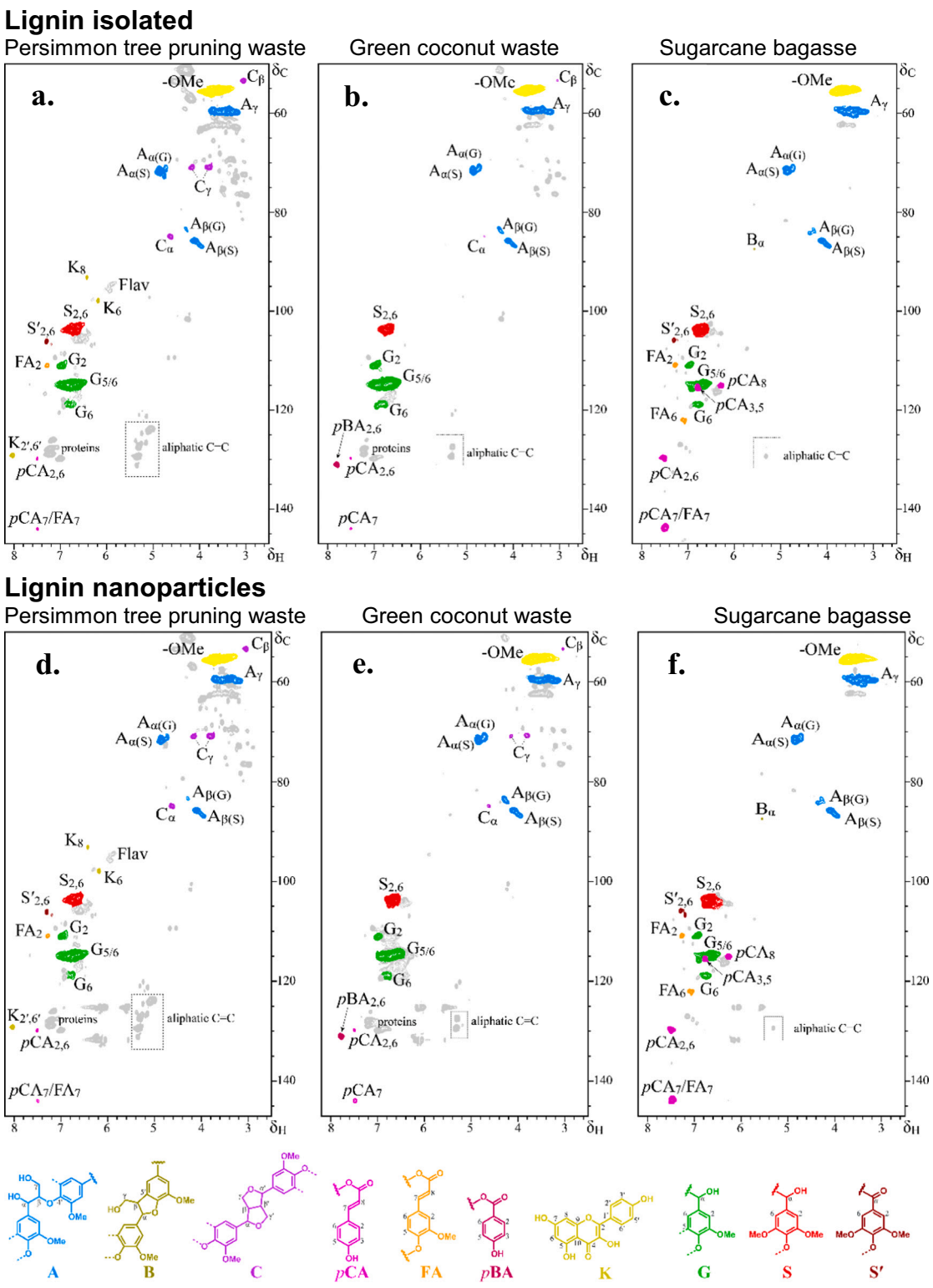

Fig. 1. 2D-HSQC NMR spectra of lignin isolated and lignin nanoparticles from (a, d) persimmon tree pruning waste, (b, e) green coconut waste, and (c, f) sugarcane bagasse. The main identified lignin structures are depicted at the bottom (A: β-*O*-4′ alkyl-aryl ethers; B: β-5′ phenylcoumarans; C: β-β' resinols; G: guaiacyl units; S: syringyl units; S′: Cα-oxidized syringyl units; FA: ferulates; *p*BA: *p*-hydroxybenzoates; *p*CA: *p*-coumaric acid; K: kaempferol). (d) 2D-HSQC NMR semiquantitative analysis of the lignin bonds and structural units, as well as FA, *p*CA, *p*BA, and kaempferol moieties in the lignins extracted from persimmon tree pruning waste, green coconut waste, and sugarcane bagasse.

chosen for the process was successful. Sequential pre-treatment with dilute acid was efficient in removing the easily hydrolysable hemicelluloses (40 %) in the first stage - washing - and dilute acid to remove the difficult to hydrolyse hemicelluloses (50–60 %) - washing and, finally, alkaline delignification followed by acid precipitation made it possible to obtain lignin for the tests to continue. This is a combined extractive pre-treatment widely used in the dissolving pulp industry (e.g. The Navigator Company, Portugal). Furthermore, this pre-treatment

makes it possible for all the stages to be carried out under very mild conditions of thermal severity, in order to prevent saccharide degradation and the formation of furanics, which react with the lignin and cause it to recondense.

3.2. Optimisation of lignin nanoparticles (LNPs) synthesis

To determine the optimal conditions for synthesizing lignin nanoparticles (LNPs), a study was conducted by varying three parameters during antisolvent precipitation: the antisolvent addition rate, the initial lignin concentration, and the pH value of the antisolvent. This process aimed to identify conditions that maximize particle uniformity, stability, and yield.

The selection of solvent mixtures and their proportions was based on preliminary tests conducted with the lignins under study. The aim was to identify solvents capable of dissolving >95 % of the freeze-dried lignin while prioritising options with lower toxicity. During testing, various solvents reported in the literature were evaluated, including DMSO, dioxane, methanol, and alkaline water. However, the results indicated that the lignins in this study showed the best solubility in a solution composed of 90 % acetone, 6 % ethanol, and 4 % water.

In the final dispersion, water accounted for 90.4 % of the total volume, as the mixture consisted of one part lignin solution (containing 4 % water) to nine parts antisolvent solution (water at pH 2). For stability analysis, LNP dispersions were not freeze-dried. After mixing the antisolvent with the lignin solution, the dispersions were stored in the dark at 5 °C. For DLS analysis, stable samples were stirred for 10 min, and aliquots of the dispersion were taken and diluted 10 to 20 times in deionised water at pH 2 for analysis.

3.2.1. Effect of antisolvent addition rate

Fig. 2 presents the hydrodynamic diameter (HDD), dispersity (Đ), and zeta potential (ζ-potential) of LNPs synthesized with 10 mg·mL^{-1} lignin, antisolvent at pH 4, and varying addition rates (25 to 250 µL·s^{-1}). Particle Size and Uniformity showed that increasing the antisolvent addition rate decreased both HDD and Đ. The smallest particles and highest homogeneity were observed at 250 µL·s^{-1} (e.g., HDD: 335 ± 5 nm for persimmon, 242 ± 10 nm for coconut, and 287 ± 12 nm for sugarcane; Đ: 0.084 ± 0.055, 0.100 ± 0.05, and 0.014 ± 0.011, respectively).

With regard to stability, it was found that slow addition rates (≤ 100 µL·s^{-1}) led to precipitate formation, whereas faster rates (150–250 µL·s^{-1}) resulted in stable dispersions. This behavior likely stems from slower addition facilitating agglomeration, consistent with previous findings [55]. In relation to the surface charge, the ζ potential varied minimally with the addition rate (−30 to −40 mV), indicating stable colloidal systems. Based on these findings, 250 µL·s^{-1} was selected as the optimal addition rate for producing uniform, stable LNPs with desirable size (240–335 nm), dispersity (0.080–0.100), and ζ-potential (−32 to −40 mV).

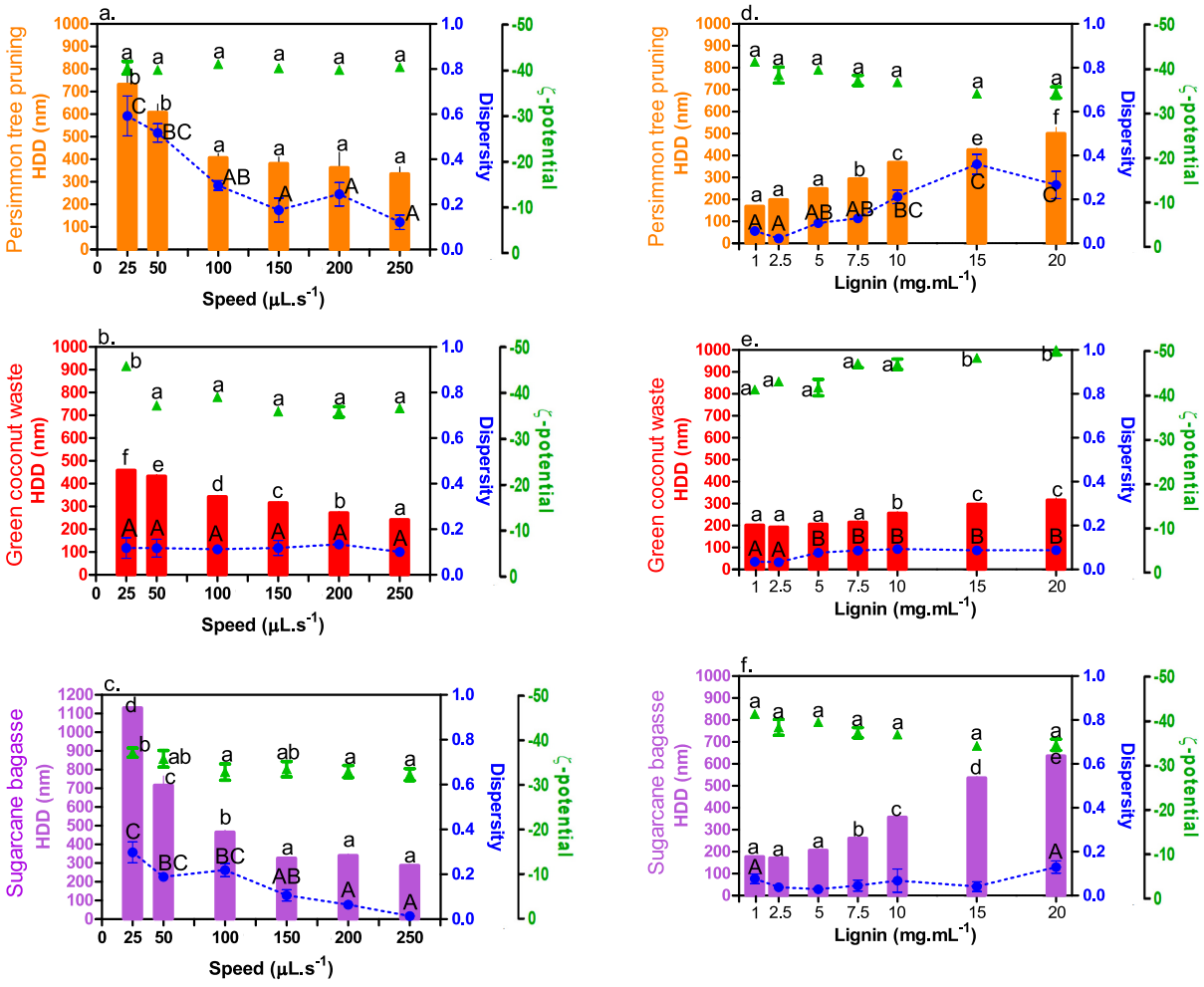

Fig. 2. Hydrodynamic diameter (HDD), dispersity (Đ), and zeta potential (ζ-potential) of lignin nanoparticles from persimmon tree pruning waste, green coconut waste, and sugarcane bagasse prepared by antisolvent precipitation by varying the addition rate of the antisolvent or the initial lignin concentration. The results are expressed as mean ± standard error. The different lowercase or uppercase letters indicate statistically significant differences (ANOVA and Tukey's test, $p \leq 0.05$) between the results obtained by the addition rate of the antisolvent for HDD, Đ, or ζ-potential.

The HDD of nanoparticles is influenced by the antisolvent addition rate. A slower addition rate allows for more precise control of nucleation and growth, resulting in smaller and more uniform particles, whereas a faster rate may lead to larger particles due to abrupt supersaturation and aggregation. Additionally, a slower antisolvent addition rate tends to result in lower Đ values, indicating a narrower size distribution, as nucleation and particle growth occur in a more controlled manner. Regarding zeta potential, a slower addition rate may lead to nanoparticles with a higher surface charge, resulting in a higher ζ-potential and, consequently, greater stability.

3.2.2. *Effect of initial lignin concentration*

The influence of lignin concentration (1–20 mg·mL^{-1}) on HDD, Đ, and ζ-potential was evaluated at 250 μL·s^{-1} and pH 4 (Fig. 2d–f). A direct correlation was observed between lignin concentration and particle size, with greater increases for persimmon and sugarcane lignins (e.g., HDD: 169 ± 3 nm to 500 ± 50 nm for persimmon; 177 ± 7 nm to 636 ± 42 nm for sugarcane). Đ remained consistent across concentrations except at the highest concentrations of persimmon lignin (15 and 20 mg·mL^{-1}). Concentrations ≥7.5 mg·mL^{-1} led to aggregation, reducing stability after 24 h at 5 °C (Supplementary material S1).

The ζ-potential remained below −30 mV, with some variations for higher coconut lignin concentrations (e.g., −41 ± 1 mV at 1 mg·mL^{-1} to −50 ± 2 mV at 20 mg·mL^{-1}). Considering stability and uniformity, 5 mg·mL^{-1} was selected as the optimal concentration, yielding LNPs with sizes of 200–250 nm, Đ between 0.022 and 0.076, and ζ-potential of −32 to −41 mV.

These data indicate that the initial lignin concentration also affects the HDD. Higher concentrations may lead to the formation of larger nanoparticles due to increased aggregation, while lower concentrations can result in smaller, more stable particles. Higher lignin concentrations can also increase Đ, as there is a greater likelihood of aggregation and the formation of particles with varying sizes. Additionally, higher lignin concentrations may reduce the ζ-potential due to increased aggregation, which decreases the electrostatic repulsion between particles.

3.2.3. *Effect of antisolvent pH*

The impact of pH (2−12) on LNP formation was assessed at 5 mg·mL^{-1} lignin and 250 μL·s^{-1} addition rate (Fig. 3a–c). HDD decreased significantly from over 2000 nm at pH 2 to <250 nm at pH 4. Beyond pH

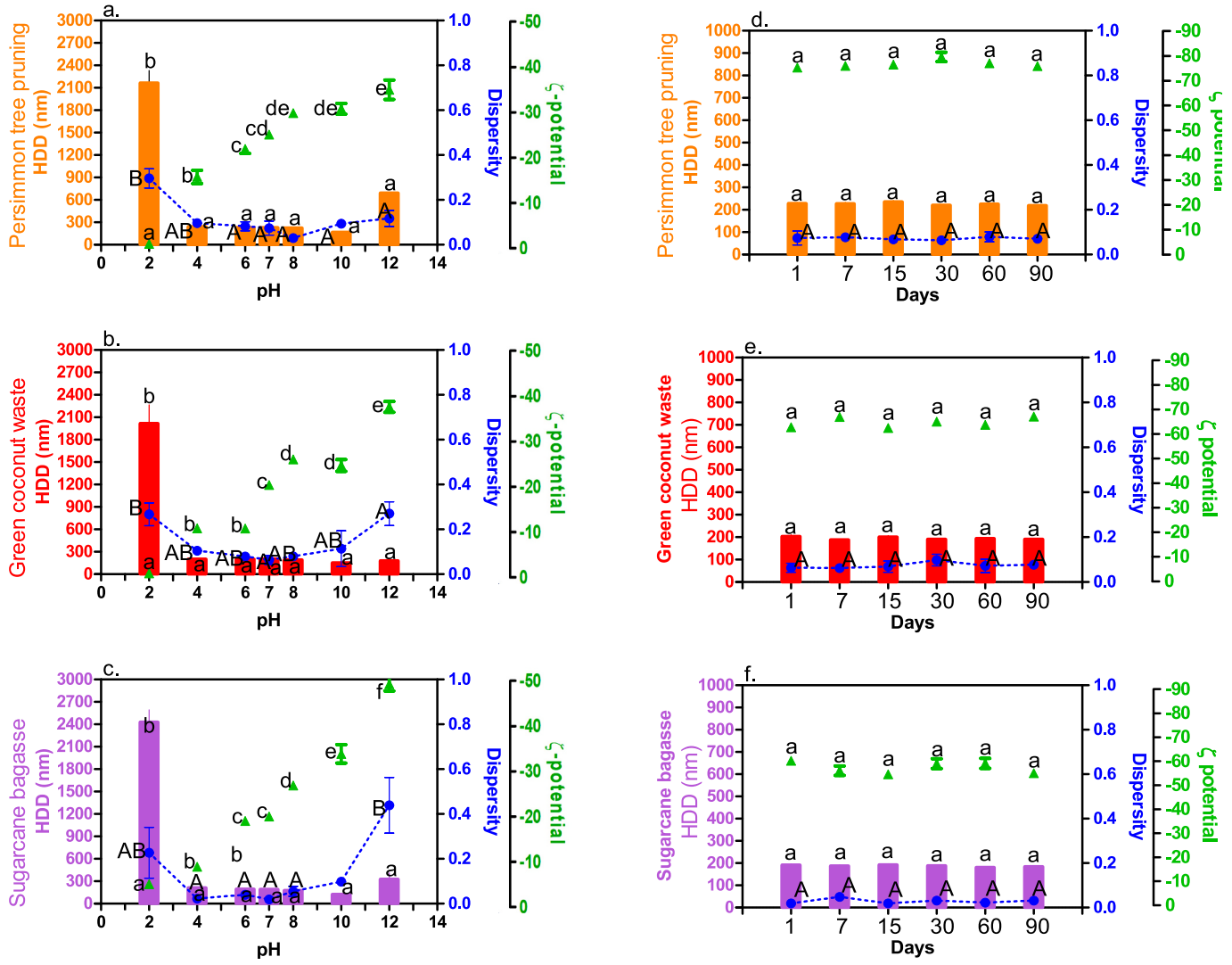

Fig. 3. Hydrodynamic diameter (HDD), dispersity (Đ), and zeta potential (ζ-potential) of lignin nanoparticles from different biomasses prepared by antisolvent precipitation by varying the pH of the antisolvent (a-f) and stability of lignin nanoparticles prepared by the optimal condition of the antisolvent precipitation evaluated for 90 days (g, h and i), stored in static mode at 5 °C. Above the plots are photographs of the dispersions the day after particle synthesis (a, c and e), stored in static mode at 5 °C. The results are expressed as mean ± standard error. The different lowercase or uppercase letters indicate statistically significant differences (ANOVA and Tukey's test, $p \leq 0.05$) between the results obtained by the addition rate of the antisolvent for HDD, Đ, or ζ-potential.

4, particle sizes remained consistent (<250 nm), but Đ increased for coconut and sugarcane lignins at pH 12, likely due to ionic interactions. The ζ-potential shifted from net positive or near-neutral values at pH 2 to strongly negative at pH 12 (−57 ± 5 mV for persimmon, −55 ± 11 mV for coconut, and − 84 ± 8 mV for sugarcane). Precipitation was observed at pH 2, while stable dispersions persisted at pH 4–8. At pH ≥ 10, brighter suspensions indicated enhanced dispersion or surface modification [54]. Under more alkaline conditions, lignin solubilisation occurred; therefore, there is a single crystalline phase.

A strong variation of particle size was observed with changes in pH was increased might be related to the different ionic charge. At low pH values, the protons interact with the hydroxyls present in the phenolic compounds, making larger aggregates possible, while at more alkaline pH values there should be repulsion of the charges of the phenolic compounds.

The differences observed between the three lignin particles charge at pH 12 are most likely related with the different composition of each lignin extract. Images of the suspensions one day after particles synthesis showed that only the LNPs obtained at pH 2 lost their stability highlighted by the formation of a precipitate at the bottom of the vial. No differences (absence of precipitate, colour, and turbidity) were observed for the particles obtained at pH 4, 6 and 8. However, when the pH of the dispersion was increased to 10 and 12, a brightening of the colour and a decrease on suspension turbidity was observed. This could indicate an improved dispersion of the nanoparticles and/or modification or dissolution of their surface [54]. An increase of pH to values ≥10 might have changed the structure or enhanced the dispersion of the nanoparticles in the medium, promoting the translucent character of the suspension.

Based on these findings, neutral pH (pH 7) was selected as optimal, yielding homogeneous, stable dispersions.

Also, these data indicate that the pH of the antisolvent significantly influences the size and stability of lignin nanoparticles. Under extreme pH conditions (highly acidic or basic), the HDD tends to increase due to the ionisation of lignin's functional groups (hydroxyl and carboxyl), affecting its solubility and promoting aggregation. In these conditions, depolymerisation or aggregate formation may occur, resulting in higher dispersity (Đ) and greater particle size heterogeneity. pH control is crucial for obtaining uniform and stable nanoparticles. At pH levels where functional groups are ionised (such as carboxyl groups in a basic medium), the ζ-potential increases, enhancing colloidal stability through electrostatic repulsion. Conversely, at pH levels near the isoelectric point of lignin, the ζ-potential approaches zero, reducing electrostatic repulsion and leading to nanoparticle aggregation.

Furthermore, lignin undergoes different ionisation patterns depending on the pH. Cationic and anionic lignin can have distinct effects on nanoparticle properties due to their opposite surface charges. Anionic lignin, for example, may promote greater electrostatic repulsion between particles, resulting in smaller and more stable nanoparticles. In contrast, cationic lignin may interact differently with the solvent or antisolvent, potentially leading to increased aggregation. These differences influence the nanoprecipitation process and the final properties of the nanoparticles.

Anionic lignin can form more hydrogen bonds (H-bonding) with the aqueous medium or other molecules, which may enhance nanoparticle stability and reduce aggregation. This is supported by FTIR data (Fig. 5), where the presence of a broad band around 3400–3200 cm^{-1} suggests the existence of hydrogen bonding between lignin hydroxyl groups and water molecules or other functional groups.

3.2.4. Optimal conditions for LNP synthesis and yields

Based on the results, the optimal synthesis conditions were initial lignin concentration: 5 $mg{\cdot}mL^{-1}$antisolvent addition rate: 250 $\mu L{\cdot}s^{-1}$ and antisolvent pH: **7**. These conditions produced LNPs with HDD between 200 and 230 nm, Đ of 0.020–0.080, and ζ-potential from −33 to −42 mV. LNP yields varied depending on lignin source: 30.8 ± 1.3 % (persimmon), 25.9 ± 0.4 % (coconut), and 28.6 ± 1.2 % (sugarcane). These results align with previous studies reporting yields between 10 and 50 % [5,16]. The production of lignin nanoparticles (LNPs) faces challenges that result in relatively low yields, typically ranging from 10 % to 50 %. These challenges stem from the complex and variable chemical structure of lignin, its diverse plant sources, and the intricacies of the nanoparticle formation process. If the lignin has an irregular, cross-linked polymeric structure, this can limit its ability to self-assemble uniformly into nanoparticles. During the lignin filtering process, part of the molecules can be retained on the filter. This was observed during the experiments in this study. Lignins with a higher degree of cross-linking (e.g. due to high guaiacyl content or extensive C—C and C-O-C bonds) often have reduced solubility and reactivity, thus hindering the efficient formation of nanoparticles [5].

The chemical composition of lignin varies with plant sources, particularly in the proportions of syringyl (S), guaiacyl (G), and *p*-hydroxyphenyl (H) units. This variability influences lignin's solubility, reactivity, and emulsification behavior, all critical factors for nanoparticle production [30].

During the antisolvent precipitation process, suboptimal conditions—such as slow antisolvent addition rates, high lignin concentrations, or inadequate pH—can lead to the formation of larger aggregates or precipitates. These aggregated particles are typically removed during purification, reducing the overall yield of well-formed LNPs. Additionally, hydrophobic or poorly soluble lignin components, like high molecular weight fractions or strongly condensed structures, may not participate in nanoparticle formation, remaining as residues or insoluble fractions excluded from the final product [38].

The reported yields of LNPs reflect these challenges and vary due to differences in experimental protocols, lignin sources, and processing conditions. For instance, lignin extracted using alkaline methods often produces higher yields of LNPs compared to those obtained through kraft or organosolv processes, owing to differences in solubility and the availability of functional groups [40]. Addressing these challenges requires a comprehensive understanding of lignin's structural variability and the development of optimised processing techniques to enhance LNP production efficiency.

3.3. Characterization and formation mechanism of LNPs

The morphology of the lignins and their nanoparticles was evaluated by FE-SEM (Fig. 4).

The three lignins presented a morphology of crystals (Fig. 4 A, B and C), while the LNPs presented spherical hollow nanostructures, which can be found dispersed or aggregated in small clusters. In the LNPs produced with lignin from persimmon pruning waste and sugarcane bagasse, the arrows show that the LNPs are actually capsules, where the structure has burst and you can see that the particles are hollow inside, which is an advantage for encapsulating compounds.

The diameter of the LNPs varied according to the lignin source: 130 ± 35 nm for the persimmon tree, 168 ± 51 nm for green coconut, and 192 ± 70 nm for sugarcane. It is noteworthy that the micrographs showed smaller diameters than those obtained by DLS. These differences are related with the particularities of each technique [41]. Studies with alkaline lignins have yielded LNPs with diameters ranging from 45 to 250 nm and spherical, hollow, or non-spherical morphology dispersed in aggregates [8,24,42]. It is important to note that even after 90 days, the morphologies were maintained, indicating the stability of the formation of LNPs (Fig. 4 G to I).

The LNPs synthesized by the optimised precipitation condition in antisolvent were analysed by 2D-NMR (Fig. 1d to f) and FT-IR (Fig. 5). The HSQC spectra of the LNPs showed strong overlap with the spectra of the corresponding lignins (Fig. 1 a, b and c), indicating high preservation of the chemical and structural composition of the lignins. The lignins had a salmon colour. Only a few new signals were observed in the 2D-NMR spectrum of the LNPs (next to the aliphatic C═C signals,

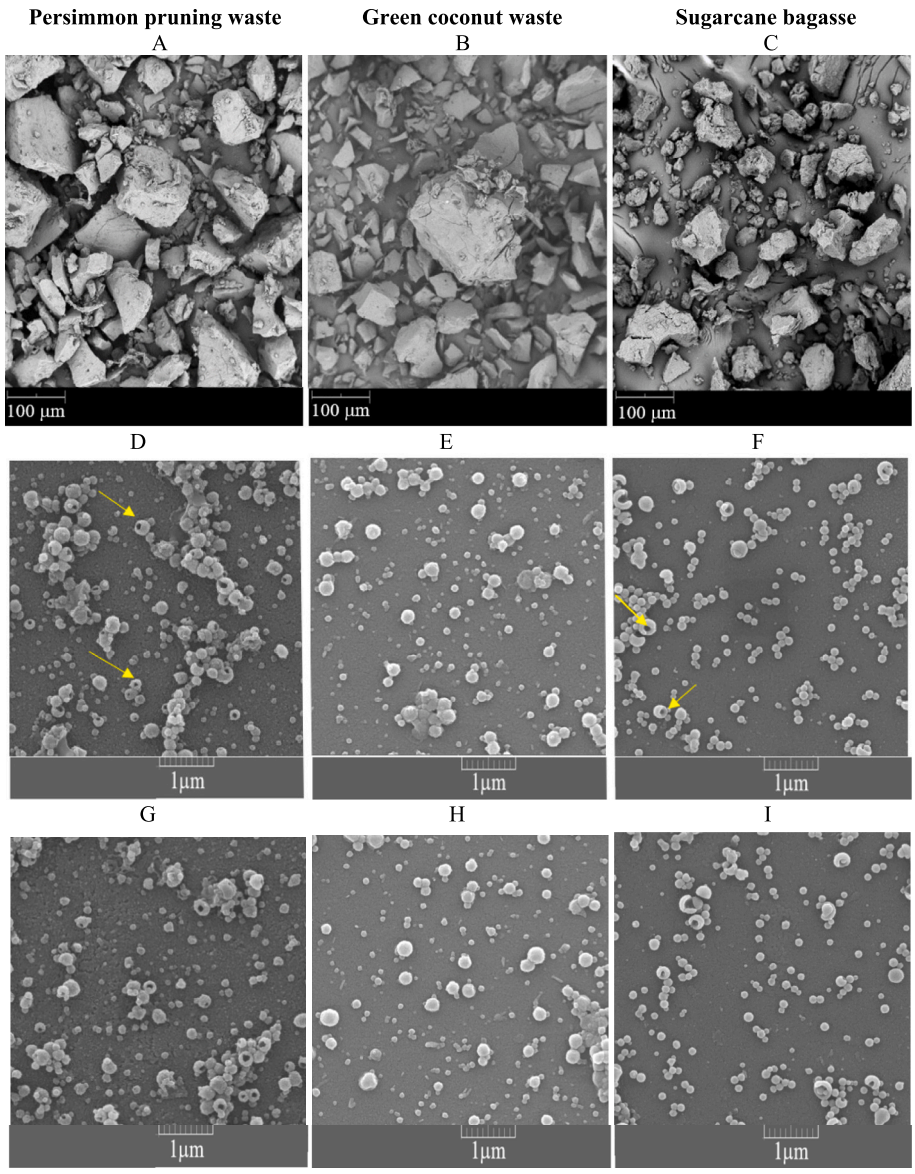

Fig. 4. FE-SEM micrographs of lignins and lignin nanoparticles (LNPs) from persimmon tree pruning waste (A, D), green coconut waste (B, E) and sugarcane bagasse (C, F). The LNPs were prepared using the optimised conditions (initial lignin concentration of 5 mg·mL^{-1}, antisolvent at pH 7, and antisolvent addition rate of 250 µL·s^{-1}).

between δ_C 125–135), which were attributed to contamination signals.

The FT-IR spectra of the lignins and correspondent LNPs showed similar absorption patterns, indicating that the structure of the lignins was not significantly altered during the preparation of the LNPs. Bands characteristic of the axial vibration of the -OH group (3400–3200 cm^{-1}) were observed (Fig. 5) due to the presence of hydroxyl groups in the aromatic and aliphatic regions of the lignin units [56]. Bands assigned to the axial vibrations of the C═O group (1700 cm^{-1}) and -CH of the -CH_2- and -CH_3 groups in the aliphatic region (2960–2850 cm^{-1}) were identified, both of which are present in the side chains of the phenylpropanoid compounds [43]. Bands corresponding to axial and/or angular vibrations of C═C (1600 and 1510 cm^{-1}) and -CH groups of aromatic rings (1424 and 1110 cm^{-1}) and H deformations in arenes (900–750 cm^{-1}) were also observed. The lignin and LNP samples showed two bands characteristic of the C-O-C bond of aromatic ethers (1275–1200 cm^{-1}), attributed to the methoxy groups (-O-CH_3) conjugated to the aromatic ring of the G and S-lignin units [43,44]. The FT-IR spectra of the lignins and LNPs showed similar absorption patterns, indicating that the structure of the lignins was not significantly altered during the preparation of the LNPs, and corroborated the 2D-NMR data. It is also worth noting that analyses were carried out after 60 and 90 days of storage and curves with the same profiles at the initial time were verified, indicating that there was no change in the lignin during these time intervals.

Despite there is no consensus in literature about the formation mechanism of LNPs, it is believed that the formation of this type of nanoparticles is associated with the amphiphilic nature of lignins with hydrophobic (phenolic groups) and hydrophilic (mainly represented by hydroxyl and methoxyl groups) moieties which can drive the self-organization of the macromolecules into nanostructures [3,13]. In this study, it is proposed that when the antisolvent is incorporated into the lignin solution, phenylpropanoids with higher molecular weight chemical structures (e.g., syringylacetone, propenylsyringol, eugenol, and vinylsyringol), self-organize in a central backbone through non-covalent bonds between their functional groups (mainly hydrogen bonds between the hydroxyl and methoxyl groups). This supramolecular structure presents their hydrophobic moieties facing inwards while their hydrophilic moieties are oriented to the surface of the structure. At the same

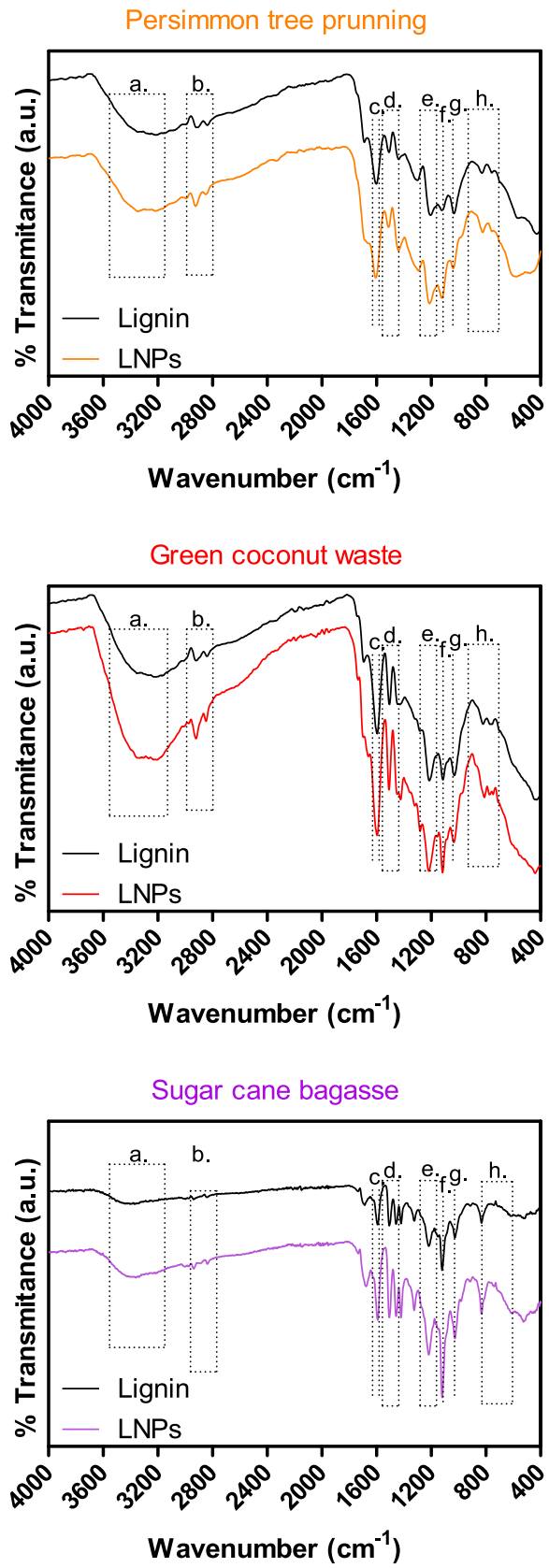

Fig. 5. FT-IR spectra of lignins and their respective lignin nanoparticles. The main identified lignin structures are depicted at the bottom (a: 3400–3200 cm^{-1}; b: 2960–2850 cm^{-1}; c: 1600 cm^{-1}; d: 1450–1550 cm^{-1}; e: 1275–1200 cm^{-1}; f: 1424 cm^{-1}; g: 1110 cm^{-1}; h: 900–750 cm^{-1}).

time, the phenylpropanoids with smaller molecular structures (for example, syringol, guaiacol, 4-methylsyringol, and 4-methylguaiacol), which are present in higher proportions, tend to aggregate to this structure through non-covalent interactions (hydrogen bonds, van der Waals force, and interactions of π-π aromatic orbitals), with their hydrophobic and hydrophilic regions facing inward and toward the surface, respectively. This mechanism of association between lignin units, either by filling or overlapping, generates a dense surface layer and forms solid nanostructures. Thus, the gradual addition of the antisolvent induces the self-assembly and precipitation of lignin into nanostructures based on the nucleation mechanism that depends on a central structure coated or filled by a dense surface layer of phenylpropanoids, minimising the surface area in contact with the antisolvent phase [5,17].

With respect to the morphology of LNPs, studies suggest that lignin molecules aggregate in the spherical conformation to maximize the π-π interactions between their aromatic hydrophobic regions, while the hydroxyl and carboxyl groups move to the interface to form effective hydrogen bonds with water [16,45]. However, in the hollow sphere conformation, the formation of vesicle-like structures would increase the density of intermolecular interactions between the hydrophilic regions of the lignin and the water on both the inner and outer surfaces. Alternatively, it is also possible that the hollow spheres are formed by the evaporation of water during sample preparation for electron microscopy analysis [16]. Fig. 6 relates different sources of lignin to the formation of LNP and how the source of lignin affects the size and structure of LNP.

3.4. UV–vis absorption performance and thermal properties of LNPs

The UV–Vis absorption spectra (230–700 nm) of the lignins and their respective LNPs are shown in Fig. 7. Although UV absorption spectra are typically measured using solutions in which the substance is fully dissolved in a solvent, this study employed dispersions of lignin and LNPs. This approach was chosen because dispersions better represent the form in which these materials are likely to be used in future products, such as sunscreens. While it is acknowledged that suspensions may contain undissolved particles that scatter light, potentially leading to less precise measurements, using solvents could compromise the structural integrity of the LNPs, thereby introducing inaccuracies in the data.

According to the methodology used in this work, we found that the absorption pattern in the UV–Vis region is similar for all samples, indicating that the chemical composition of the lignins is preserved in the LNPs. The samples show absorption in the UVA (280–380 nm), UVB (280–320 nm), and UVC (230–280 nm) regions with an absorption maximum at 260 nm. However, they show low absorption in the Vis region (380–700 nm). This is because the electronic transitions that occur in the aromatic rings and the conjugated bonds of the lignin units require more energy than visible light can provide. Lignins absorb UV radiation where the energy is enough to promote n-π* transitions of the conjugated phenolic groups and π-π* transitions of the aromatic rings [46,47].

The n-π^* and π-π^* transitions are associated with functional groups containing atoms with lone electron pairs, such as phenolic hydroxyl and methoxy groups. In the phenolic hydroxyl groups of lignin, the lone electron pairs on oxygen promote absorption in the 280–300 nm range. In LNPs, structural reorganization increases the exposure or local concentration of these groups, enhancing absorption. Methoxy groups, abundant in lignins with high guaiacyl and syringyl unit content, also contribute to these transitions, absorbing at similar wavelengths due to the lone electron pairs on oxygen [47,48].

Conjugated double bonds in aromatic rings contribute to n-π^* and π-π^* transitions, with intense absorption in the 200–250 nm region, which is highly sensitive to conjugation and molecular organization. The formation of LNPs can improve the efficiency of these transitions due to increased structural organization. Carbonyl groups, present in oxidized lignins, also absorb in nearby ranges, and their reorganization in

Lignin sources	Persimmon pruning waste	Green coconut waste	Sugarcane bagasse
Trends in LNP formation	**High G content** Reduced solubility, moderate particle size.	**High H content** Poor emulsification, larger particles.	**Balanced S and G content** High solubility, smaller, uniform particles.
Output nanoparticles	Medium-sized, moderately uniform particles.	Larger, less uniform particles.	Small, uniform particles.
Nanoparticles representation	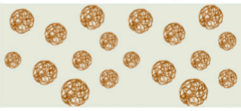		

Fig. 6. Schematic representation of the different sources of lignin and their effect on the formation and effects on the size and structure of LNP.

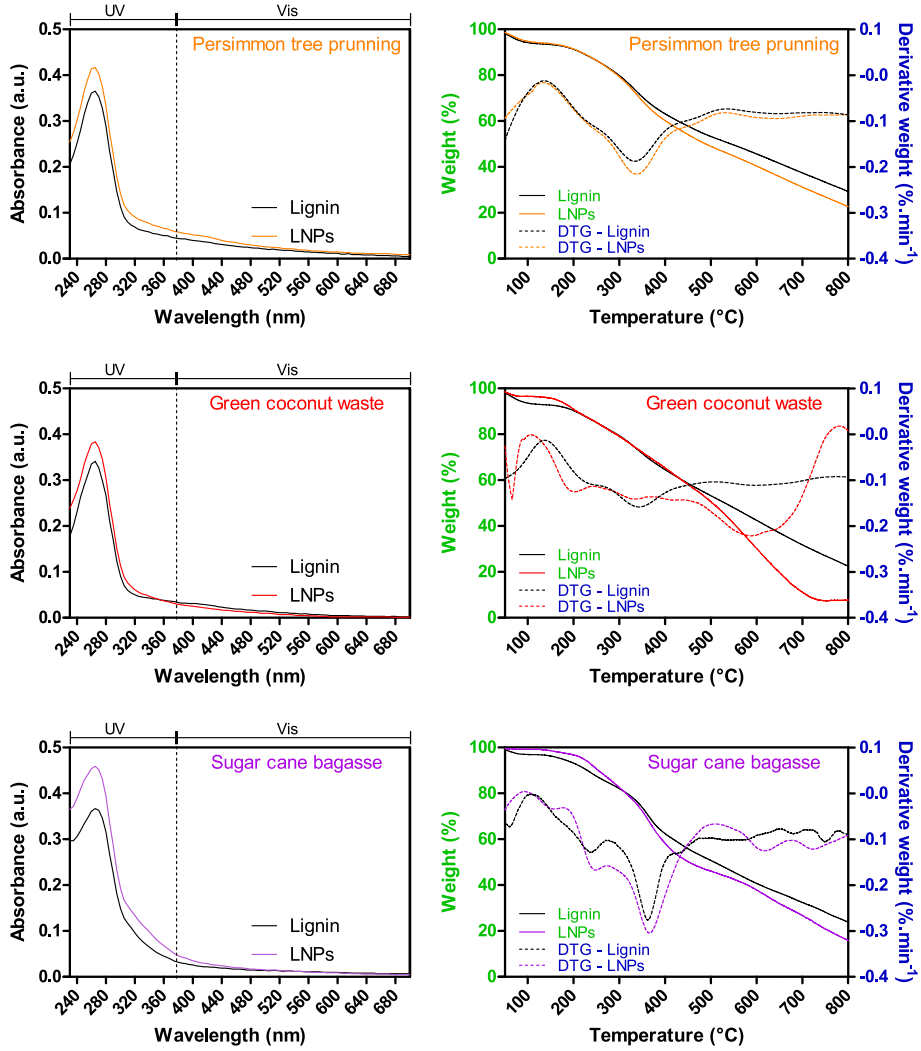

Fig. 7. UV–Vis absorption spectra and thermogravimetric (TG) and derived thermogravimetric (DTG) curves of lignin and lignin nanoparticles from different biomasses.

nanoparticle form can enhance accessibility to UV light, resulting in greater absorption intensity [47,48].

Although the formation of LNPs does not chemically alter functional groups, it modifies their structural organization, local concentration, and interaction with light. This redistribution of phenolic, methoxy, and carbonyl groups, as well as conjugated double bonds, increases the efficiency of n-π^* and π-π^* transitions, improving optical properties without altering the chemical composition [47,48].

Lignins with higher S/G ratio (sugarcane bagasse and persimmon pruning waste) had the highest absorptions in the UV region. Moreover, the sugarcane bagasse LNPs, which are rich in *p*-coumarates that have strong UV absorption [49,50], had higher UV absorption than the persimmon pruning waste LNPs. Therefore, a direct proportional relationship was observed between S/G ratio and *p*-coumarate content in lignins and their UV absorption capacity.

p-coumarates, derived from p-coumaric acid, are aromatic compounds with a single −OH group and no methoxy groups. Their conjugated side chain (C=C − C=O) enhances n-π^* and π-π^* transitions, contributing to strong UV absorption [50],. This effect is amplified in lignin nanoparticles (LNPs), where structural organization increases the exposure of p-coumarates to UV light. While lignins with high S unit content exhibit enhanced UV absorption due to the methoxy groups facilitating n-π^* and π-π^* transitions, in sugarcane bagasse, the conjugated system of p-coumarates compensates for the absence of methoxy groups, resulting in strong UV absorption [51].

The superior UV absorption capacity of lignins with a high S/G ratio is linked to their molecular structure. Syringyl (S) units, with two methoxy groups on the aromatic ring, promote greater electronic conjugation compared to guaiacyl (G) units, which have only one methoxy group. This increased methoxylation enhances UV absorption, making lignins with higher S unit proportions particularly effective for UV protection applications [49,50].

The improved UV absorbance of lignins in nanoparticle form (LNPs), despite unchanged chemical composition, can be attributed to changes in physical and structural properties. The nanoparticle formation process increases lignin's specific surface area, exposing more chromophore groups, such as aromatic rings and other UV-absorbing functional groups, to UV light. Additionally, the reorganization or concentration of functional groups during nanoparticle formation enhances UV absorption efficiency. Nanoparticles may also introduce a physical effect by influencing light scattering, further contributing to the observed improvement in UV absorbance.

Analysing the thermogravimetric (TG) and derivative (DTG) curves of lignin and LNPs one can observe that lignins and LNPs underwent an initial mass loss of about 5 % at 50–60 °C, which can be attributed to the desorption of moisture, although the nanoparticles were lyophilised previously [52]. A second thermal decomposition stage was observed between 180 and 220 °C, associated with the elimination of formic acid, formaldehyde, carbon dioxide and water, resulting from the degradation of phenylpropane side chains. The largest thermal decomposition stage (~40 %) occurred in the temperature range of 275–500 °C for the persimmon tree and sugarcane samples. This is due to the rupture of the lignin structure, where monomeric phenols would be released into the gas phase by the cleavage of bonds between phenolic hydroxyl units, carbonyl, benzyl, and hydroxyl groups, along with the decomposition of carbohydrates [53]. Green coconut lignin also exhibited the maximum decomposition stage between 300 and 400 °C, but this stage shifted to the range between 500 and 720 °C for the LNPs, indicating a higher resistance to thermal degradation than their original lignin. Between 600 and 800 °C, a residual mass loss of about 20–35 % occurred, corresponding to the formation of non-volatile solids and ash [52]. The final residue was lower for LNPs than for lignin. Therefore, our results suggest that LNPs have higher thermal stability than the corresponding lignin.

3.5. Stability of lignin nanoparticles during storage

The LNPs were stored in static mode at 5 °C for 90 days and characterized by HDD, Đ, and ζ-potential at different time points (Fig. 3d to f). The term "stored in a static model" refers to the fact that the LNP dispersions were not freeze-dried and remained undisturbed during storage. After mixing the antisolvent with the lignin solution, the dispersions were kept in the dark at 5 °C in a static state (without agitation). They were neither diluted nor concentrated before analysis, maintaining these conditions until DLS measurement. For DLS analysis, stable samples were stirred for 10 min, and aliquots were taken and diluted 10 to 20 times in deionised water at pH 2 before analysis.

Few differences were observed for all the parameters evaluated and for all the types of lignins, indicating that the LNPs were stable in the aqueous dispersion without any tendency to agglomerate or sediment. This behavior may be due to the presence of hydroxyl and methoxyl groups on the surface of the LNPs, which give interactions so that the LNPs remain suspended in the water and prevent particle coalescence [14]. Moreover, the negative zeta potential of LNPs implies electrostatic repulsion between them, which also helps their stability [53]. These results are in agreement with other studies that have reported the formation and stability of LNPs in aqueous media [14].

Although the production of LNPs has been satisfactory, we recognise the environmental concerns regarding the use of solvents such as acetone and have therefore taken a careful approach to the choice of concentrations and solvent recovery in order to minimise the environmental impact. In a possible scale-up application, the use of closed systems and solvent recovery techniques are strategies we plan to investigate further to ensure an environmentally sustainable process.

4. Conclusion

Lignins from various lignocellulosic sources can serve as sustainable polymeric matrices to produce nanostructures via antisolvent precipitation. The resulting LNPs were spherical, stable in water, and exhibited greater UV absorption and thermal stability compared to the original lignins. The UV absorption and degradation correlated with the S/G ratio. The nucleation process, forming a dense phenylpropanoid surface layer, did not alter the lignins' chemical composition. These methods enable LNP production from various plant sources for diverse applications, though more research is needed for process scalability and to explore further uses.

CRediT authorship contribution statement

Ricardo Marchezan Farias de Mesquita: Writing – original draft, Methodology, Investigation, Formal analysis, Data curation, Conceptualization. **Willian Daniel Hahn Schneider:** Writing – review & editing, Supervision, Methodology, Formal analysis, Data curation. **Vinicius Longo:** Methodology, Formal analysis. **Henrique Macedo Baudel:** Writing – review & editing, Methodology, Funding acquisition, Formal analysis, Conceptualization. **Eduardo Diebold:** Writing – review & editing, Funding acquisition, Data curation. **Jorge Rencoret:** Writing – review & editing, Methodology. **Ana Gutiérrez:** Writing – review & editing, Methodology. **Artur Cavaco-Paulo:** Writing – review & editing, Supervision. **Artur Ribeiro:** Writing – review & editing, Supervision, Methodology, Investigation, Formal analysis. **Marli Camassola:** Writing – review & editing, Supervision, Resources, Project administration, Funding acquisition, Conceptualization.

Declaration of competing interest

The authors declare that they have no known competing financial interests or personal relationships that could have appeared to influence the work reported in this paper.

Acknowledgements

This work was supported by Brazilian National Council for Scientific and Technological Development (CNPq), process number 202536/2020-3 and 405955/2022-7 and MCIN/AEI/10.13039/501100011033 (Spanish project PID2020-118968RB-I00). This study was supported by the Portuguese Foundation for Science and Technology (FCT) under the scope of the strategic funding of UIDB/04469/2020 unit, and by LABBELS – Associate Laboratory in Biotechnology, Bioengineering and Microelectromechanical Systems, LA/P/0029/2020. A.R. thank FCT for its contract under the CEEC-Individual—4th Edition with the reference 2021.02803.CEECIND.

Appendix A. Supplementary data

Supplementary data to this article can be found online at https://doi.org/10.1016/j.ijbiomac.2025.141676.

Data availability

Data will be made available on request.

References

[1] L. Cao, I.K.M. Yu, Y. Liu, X. Ruan, D.C.W. Tsang, A.J. Hunt, Y.S. Ok, H. Song, S. Zhang, Lignin valorization for the production of renewable chemicals: state-of-the-art review and future prospects, Bioresour. Technol. 269 (2018) 465–475, https://doi.org/10.1016/j.biortech.2018.08.065.

[2] A. Naseem, S. Tabasum, K.M. Zia, M. Zuber, M. Ali, A. Noreen, Lignin-derivatives based polymers, blends and composites: a review, Int. J. Biol. Macromol. 93 (2016) 296–313, https://doi.org/10.1016/j.ijbiomac.2016.08.030.

[3] W.D.H. Schneider, A.J.P. Dillon, M. Camassola, Lignin nanoparticles enter the scene: a promising versatile green tool for multiple applications, Biotechnol. Adv. 47 (2021) 107685, https://doi.org/10.1016/j.biotechadv.2020.107685.

[4] V.K. Ponnusamy, D.D. Nguyen, J. Dharmaraja, S. Shobana, J.R. Banu, R. G. Saratale, S.W. Chang, G. Kumar, A review on lignin structure, pretreatments, fermentation reactions and biorefinery potential, Bioresour. Technol. 271 (2019) 462–472, https://doi.org/10.1016/j.biortech.2018.09.070.

[5] Z. Zhang, V. Terrasson, E. Guénin, Lignin Nanoparticles and Their Nanocomposites. Nanomaterials 11 (2021) 1336, https://doi.org/10.3390/nano11051336.

[6] C. Frangville, M. Rutkevičius, A.P. Richter, O.D. Velev, S.D. Stoyanov, V.N. Paunov, Fabrication of environmentally biodegradable lignin nanoparticles, ChemPhysChem 13 (2012) 4235–4243, https://doi.org/10.1002/cphc.201200537.

[7] S.C. Lee, T.M.T. Tran, J.W. Choi, K. Won, Lignin for white natural sunscreens, Int. J. Biol. Macromol. 122 (2019) 549–554, https://doi.org/10.1016/j.ijbiomac.2018.10.184.

[8] A.P. Richter, B. Bharti, H.B. Armstrong, J.S. Brown, D. Plemmons, V.N. Paunov, S. D. Stoyanov, O.D. Velev, Synthesis and characterization of biodegradable lignin nanoparticles with tunable surface properties, Langmuir 32 (2016) 6468–6477, https://doi.org/10.1021/ACS.LANGMUIR.6B01088/SUPPL_FILE/LA6B01088_SI_001.PDF.

[9] Sadeghifar, H., Ragauskas, A., 2020. Lignin as a UV light blocker—a review. Polymers 2020, Vol. 12, page 1134 12, 1134. doi:https://doi.org/10.3390/POLYM12051134.

[10] H. Wang, Y. Pu, A. Ragauskas, B. Yang, From lignin to valuable products–strategies, challenges, and prospects, Bioresour. Technol. 271 (2019) 449–461, https://doi.org/10.1016/j.biortech.2018.09.072.

[11] Y. Cao, S.S. Chen, S. Zhang, Y.S. Ok, B.M. Matsagar, K.C.W. Wu, D.C.W. Tsang, Advances in lignin valorization towards bio-based chemicals and fuels: lignin biorefinery, Bioresour. Technol. 291 (2019) 121878, https://doi.org/10.1016/j.biortech.2019.121878.

[12] A.J. Ragauskas, G.T. Beckham, M.J. Biddy, R. Chandra, F. Chen, M.F. Davis, B. H. Davison, R.A. Dixon, P. Gilna, M. Keller, P. Langan, A.K. Naskar, J.N. Saddler, T. J. Tschaplinski, G.A. Tuskan, C.E. Wyman, Lignin valorization: improving lignin processing in the biorefinery, Science 1979 (2014), https://doi.org/10.1126/science.1246843.

[13] M. Österberg, M.H. Sipponen, B.D. Mattos, O.J. Rojas, Spherical lignin particles: a review on their sustainability and applications, Green Chem. 22 (2020) 2712–2733, https://doi.org/10.1039/D0GC00096E.

[14] M. Morsali, A. Moreno, A. Loukovitou, I. Pylypchuk, M.H. Sipponen, Stabilized lignin nanoparticles for versatile hybrid and functional nanomaterials, Biomacromolecules 23 (2022) 4597–4606, https://doi.org/10.1021/ACS.BIOMAC.2C00840/ASSET/IMAGES/LARGE/BM2C00840_0006.JPEG.

[15] Y. Qian, X. Zhong, Y. Li, X. Qiu, Fabrication of uniform lignin colloidal spheres for developing natural broad-spectrum sunscreens with high sun protection factor, Ind. Crop. Prod. 101 (2017) 54–60, https://doi.org/10.1016/j.indcrop.2017.03.001.

[16] H. Trevisan, C.A. Rezende, Pure, stable and highly antioxidant lignin nanoparticles from elephant grass, Ind. Crop. Prod. 145 (2020) 112105, https://doi.org/10.1016/j.indcrop.2020.112105.

[17] Y. Yang, J. Xu, J. Zhou, X. Wang, Preparation, characterization and formation mechanism of size-controlled lignin nanoparticles, Int. J. Biol. Macromol. 217 (2022) 312–320, https://doi.org/10.1016/J.IJBIOMAC.2022.07.046.

[18] A.P. Richter, B. Bharti, H.B. Armstrong, J.S. Brown, D. Plemmons, V.N. Paunov, S. D. Stoyanov, O.D. Velev, Synthesis and characterization of biodegradable lignin nanoparticles with tunable surface properties, Langmuir 32 (2016) 6468–6477, https://doi.org/10.1021/ACS.LANGMUIR.6B01088/ASSET/IMAGES/LARGE/LA-2016-010883_0009.JPEG.

[19] M.L. Mattinen, J.J. Valle-Delgado, T. Leskinen, T. Anttila, G. Riviere, M. Sipponen, A. Paananen, K. Lintinen, M. Kostiainen, M. Österberg, Enzymatically and chemically oxidized lignin nanoparticles for biomaterial applications, Enzym. Microb. Technol. 111 (2018) 48–56, https://doi.org/10.1016/j.enzmictec.2018.01.005.

[20] A. Moreno, J. Liu, M. Morsali, M.H. Sipponen, Chemical modification and functionalization of lignin nanoparticles, Micro and Nanolignin in Aqueous Dispersions and Polymers: Interactions, Properties, and Applications 385–431 (2022), https://doi.org/10.1016/B978-0-12-823702-1.00003-7.

[21] M.N. Garcia Gonzalez, M. Levi, S. Turri, G. Griffini, Lignin nanoparticles by ultrasonication and their incorporation in waterborne polymer nanocomposites, J. Appl. Polym. Sci. 134 (2017) 45318, https://doi.org/10.1002/app.45318.

[22] H. Yang, Z. Shi, G. Xu, Y. Qin, J. Deng, J. Yang, Bioethanol production from bamboo with alkali-catalyzed liquid hot water pretreatment. (2018), https://doi.org/10.1016/j.biortech.2018.11.088.

[23] M. Lievonen, J.J. Valle-Delgado, M.L. Mattinen, E.L. Hult, K. Lintinen, M. A. Kostiainen, A. Paananen, G.R. Szilvay, H. Setälä, M. Österberg, A simple process for lignin nanoparticle preparation, Green Chem. 18 (2016) 1416–1422, https://doi.org/10.1039/c5gc01436k.

[24] Y. Li, X. Qiu, Y. Qian, W. Xiong, D. Yang, pH-responsive lignin-based complex micelles: preparation, characterization and application in oral drug delivery, Chem. Eng. J. 327 (2017) 1176–1183, https://doi.org/10.1016/J.CEJ.2017.07.022.

[25] R.M.F. Mesquita, J.C. Dal Prá, R.C. Fontana, S. Montipó, H.M. Baudel, E. Diebold, D.H.W. Schneider, M. Camassola, Processing of persimmon tree pruning waste through the circular economy: lignin nanoparticles and cellulosic ethanol production, Renew. Energy 238 (2025) 121932, https://doi.org/10.1016/j.renene.2024.121932.

[26] B. Hames, C. Scarlata, A. Sluiter, Determination of Protein Content in Biomass: Laboratory Analytical Procedure (LAP); Issue Date 05/23/2008, 2008.

[27] A. Sluiter, R. Ruiz, C. Scarlata, J. Sluiter, D. Templeton, Determination of Extractives in Biomass: Laboratory Analytical Procedure (LAP); Issue Date 7/17/2005, 2008.

[28] A. Sluiter, B. Hames, R. Ruiz, C. Scarlata, J. Sluiter, D. Templeton, Determination of Ash in Biomass: Laboratory Analytical Procedure (LAP); Issue Date: 7/17/2005, 2008.

[29] A. Sluiter, B. Hames, R. Ruiz, C. Scarlata, J. Sluiter, D. Templeton, D. Crocker, NREL/TP-510-42618 analytical procedure - determination of structural carbohydrates and lignin in biomass, Laboratory Analytical Procedure (LAP) 17. doi:NREL/TP-510-42618, 2012.

[30] J. Rencoret, P. Prinsen, A. Gutiérrez, Á.T. Martínez, J.C. Del Río, Isolation and structural characterization of the milled wood lignin, dioxane lignin, and cellulolytic lignin preparations from brewer?S spent grain, J. Agric. Food Chem. 63 (2015) 603–613, https://doi.org/10.1021/JF505808C/ASSET/IMAGES/MEDIUM/JF-2014-05808C_0007.GIF.

[31] J. Rencoret, J. Ralph, G. Marques, A. Gutiérrez, Á.T. Martínez, J.C. Del Río, Structural characterization of lignin isolated from coconut (Cocos nucifera) coir fibers, J. Agric. Food Chem. 61 (2013) 2434–2445, https://doi.org/10.1021/JF304686X/ASSET/IMAGES/LARGE/JF-2012-04686X_0005.JPEG.

[32] X. Du, M. Pérez-Boada, C. Fernández, J. Rencoret, J.C. del Río, J. Jiménez-Barbero, J. Li, A. Gutiérrez, A.T. Martínez, Analysis of lignin–carbohydrate and lignin–lignin linkages after hydrolase treatment of xylan–lignin, glucomannan–lignin and glucan–lignin complexes from spruce wood, Planta 239 (2014) 1079–1090, https://doi.org/10.1007/s00425-014-2037-y.

[33] N. Maldonado-Carmona, G. Marchand, N. Villandier, T.S. Ouk, M.M. Pereira, M.J. F. Calvete, C.A. Calliste, A. Żak, M. Piksa, K.J. Pawlik, K. Matczyszyn, S. Leroy-Lhez, Porphyrin-loaded lignin nanoparticles against Bacteria: a photodynamic antimicrobial chemotherapy application, Front. Microbiol. 17 (2020) 606185, https://doi.org/10.3389/fmicb.2020.606185.

[34] J. Rencoret, J. Ralph, G. Marques, A. Gutiérrez, Á.T. Martínez, J.C. Del Río, Structural characterization of lignin isolated from coconut (Cocos nucifera) coir fibers, J. Agric. Food Chem. 61 (2013) 2434–2445, https://doi.org/10.1021/jf304686x.

[35] A. Smit, W. Huijgen, Effective fractionation of lignocellulose in herbaceous biomass and hardwood using a mild acetone organosolv process, Green Chem. 19 (2017) 5505–5514, https://doi.org/10.1039/c7gc02379k.

[36] D. Lebedeva, S. Hijmans, A.P. Mathew, E. Subbotina, J.S.M. Samec, Waste-to-fuel approach: valorization of lignin from coconut coir pith, ACS Agric. Sci. Technol. 2 (2022) 349–358, https://doi.org/10.1021/ACSAGSCITECH.1C00248.

[37] A. Beaucamp, M. Muddasar, I.S. Amiinu, M. Moraes Leite, M. Culebras, K. Latha, M.C. Gutiérrez, D. Rodriguez-Padron, F. del Monte, T. Kennedy, K.M. Ryan, R. Luque, M.M. Titirici, M.N. Collins, Lignin for energy applications – state of the art, life cycle, technoeconomic analysis and future trends, Green Chem. 24 (2022) 8193–8226, https://doi.org/10.1039/D2GC02724K.

[38] Q. Tang, Y. Qian, D. Yang, X. Qiu, Y. Qin, M. Zhou, Lignin-based nanoparticles: a review on their preparations and applications, Polymers (Basel). 25 (2020) 2471, https://doi.org/10.3390/polym12112471.
[39] P. Figueiredo, M.H. Lahtinen, M.B. Agustin, D.M. de Carvalho, S.P. Hirvonen, P. A. Penttilä, K.S. Mikkonen, Green fabrication approaches of lignin nanoparticles from different technical Lignins: a comparison study, ChemSusChem 14 (2021) 4718–4730, https://doi.org/10.1002/cssc.202101356.
[40] W. He, W. Gao, P. Fatehi, Oxidation of Kraft lignin with hydrogen peroxide and its application as a dispersant for kaolin suspensions, ACS Sustain. Chem. Eng. 5 (2017) 10597–10605, https://doi.org/10.1021/acssuschemeng.7b02582.
[41] N. Tarannum, D. Divya, Y.K. Gautam, Facile green synthesis and applications of silver nanoparticles: a state-of-the-art review, RSC Adv. 9 (2019) 34926–34948, https://doi.org/10.1039/C9RA04164H.
[42] L. Dai, Y. Li, R. Liu, C. Si, Y. Ni, Green mussel-inspired lignin magnetic nanoparticles with high adsorptive capacity and environmental friendliness for chromium(III) removal, Int. J. Biol. Macromol. 132 (2019) 478–486, https://doi.org/10.1016/J.IJBIOMAC.2019.03.222.
[43] M.K. He, Y.L. He, Z.Q. Li, L.N. Zhao, S.Q. Zhang, H.M. Liu, Z. Qin, Structural characterization of lignin and lignin-carbohydrate complex (LCC) of sesame hull, Int. J. Biol. Macromol. 209 (2022) 258–267, https://doi.org/10.1016/J.IJBIOMAC.2022.04.009.
[44] Z. Qin, Y.X. Ma, H.M. Liu, G.Y. Qin, X. De Wang, Structural elucidation of lignin-carbohydrate complexes (LCCs) from Chinese quince (Chaenomeles sinensis) fruit, Int. J. Biol. Macromol. 116 (2018) 1240–1249, https://doi.org/10.1016/j.ijbiomac.2018.05.117.
[45] X. Rao, Yongzhuang Liu, Q. Zhang, W. Chen, Yixing Liu, H. Yu, Assembly of Organosolv lignin residues into submicron spheres: the effects of granulating in ethanol/water mixtures and homogenization, ACS Omega 2 (2017) 2858–2865, https://doi.org/10.1021/ACSOMEGA.7B00285/ASSET/IMAGES/LARGE/AO-2017-00285B_0007.JPEG.
[46] O.Y. Abdelaziz, C.P. Hulteberg, Physicochemical characterisation of technical Lignins for their potential valorisation, Waste Biomass Valoriz. 8 (2017) 859–869, https://doi.org/10.1007/S12649-016-9643-9/FIGURES/6.
[47] Kumar, A.K., Sharma, S., 2017. Recent updates on different methods of pretreatment of lignocellulosic feedstocks: a review. Bioresources and bioprocessing 2017 4:1 4, 1–19. doi:https://doi.org/10.1186/S40643-017-0137-9.
[48] Y. Li, S. Zhao, D. Hu, A.J. Ragauskas, D. Cao, W. Liu, C. Si, T. Xu, P. Zhao, K. Song, K. Kai Li, Role evaluation of active groups in lignin on UV-shielding performance, ACS Sustain. Chem. Eng. 10 (2022) 11856–11866, https://doi.org/10.1021/acssuschemeng.2c02714.
[49] González Moreno, A., de Cózar, A., Prieto, P., Domínguez, E., Heredia, A., 2022. Radiationless mechanism of UV deactivation by cuticle phenolics in plants. Nature Communications 2022 13:1 13, 1–11. doi:https://doi.org/10.1038/s41467-022-29460-9.
[50] Wulansari, A.D., Hayati, D., Long, D.X., Choi, K., Hong, J., 2023. Hydroxycinnamic acid derivatives for UV-selective and visibly transparent dye-sensitized solar cells. Scientific reports 2023 13:1 13, 1–11. doi:https://doi.org/10.1038/s41598-022-17236-6.
[51] R. Wen, S. Fu, H. Zhang, Synergy of modified lignin and p-coumaric acid for improving the function of sun-protection in sunscreen, BioResources 18 (2023) 1602–1615, https://doi.org/10.15376/biores.18.1.1602-1615.
[52] U.P. Perera, M.L. Foo, I.M.L. Chew, Synthesis and characterization of lignin nanoparticles isolated from oil palm empty fruit bunch and application in biocomposites, Sustainable Chemistry for Climate Action 2 (2023) 100011, https://doi.org/10.1016/J.SCCA.2022.100011.
[53] S. Sen, S. Patil, D.S. Argyropoulos, Thermal properties of lignin in copolymers, blends, and composites: a review, Green Chem. 17 (2015) 4862–4887, https://doi.org/10.1039/C5GC01066G.
[54] Wang, Y., Quinsaat, J.E.Q., Ono, T., Maeki, M., Tokeshi, M., Isono, T., Tajima, K., Satoh, T., Sato, S.S, Miura, Y., Yamamoto, T., 2020. Enhanced dispersion stability of gold nanoparticles by the physisorption of cyclic poly(ethylene glycol). Nature communications 2020 11:1 11, 1–12. doi:https://doi.org/10.1038/s41467-020-19947-8.
[55] A. Duval, M. Lawoko, A review on lignin-based polymeric, micro- and nano-structured materials, React. Funct. Polym. 85 (2014) 78–96, https://doi.org/10.1016/j.reactfunctpolym.2014.09.017.
[56] A. Mandak, et al., Structural characterization of lignin in wild-type versus COMT down-regulated switchgrass, Front. Energy Res. 1 (2013) 14, https://doi.org/10.3389/fenrg.2013.00014.